

Characterizing the Effects of the Juxtamembrane Domain on Vascular Endothelial Growth Factor Receptor-2 Enzymatic Activity, Autophosphorylation, and Inhibition by Axitinib

James Solowiej,[‡] Simon Bergqvist,[‡] Michele A. McTigue, Tami Marrone, Terri Quenzer, Morena Cobbs, Kevin Ryan, Robert S. Kania, Wade Diehl, and Brion W. Murray*

Pfizer Global Research and Development, La Jolla, Pfizer Inc., 10777 Science Center Drive, San Diego, California 92121.

[‡] *Equal contributors.*

Received March 26, 2009; Revised Manuscript Received June 11, 2009

ABSTRACT: The catalytic domains of protein kinases are commonly treated as independent modular units with distinct biological functions. Here, the interactions between the catalytic and juxtamembrane domains of VEGFR2 are studied. Highly purified preparations of the receptor tyrosine kinase VEGFR2 catalytic domain without (VEGFR2-CD) and with (VEGFR2-CD/JM) the juxtamembrane (JM) domain were characterized by kinetic, biophysical, and structural methods. Although the catalytic parameters for both constructs were similar, the autophosphorylation rate of VEGFR2-CD/JM was substantially faster than VEGFR2-CD. The first event in the autophosphorylation reaction was phosphorylation of JM residue Y801 followed by phosphorylation of activation loop residues in the CD. The rates of activation loop autophosphorylation for the two constructs were determined to be similar. The autophosphorylation rate of Y801 was invariant on enzyme concentration, which is consistent with an intramolecular reaction. In addition, the first biochemical characterization of the advanced clinical compound axitinib is reported. Axitinib was found to have 40-fold enhanced biochemical potency toward VEGFR2-CD/JM ($K_i = 28$ pM) compared to VEGFR2-CD, which correlates better with cellular potency. Calorimetric studies, including a novel ITC compound displacement method, confirmed the potency and provided insight into the thermodynamic origin of the potency differences. A structural model for the VEGFR2-CD/JM is proposed based on the experimental findings reported here and on the JM position in c-Kit, FLT3, and CSF1/cFMS. The described studies identify potential functions of the VEGFR2 JM domain with implications to both receptor biology and inhibitor design.

Receptor tyrosine kinases (RTK)¹ such as the vascular endothelial growth factor receptor-2 (VEGFR2, KDR) have become important and productive drug discovery targets due to their central role in many biological processes (1–5). VEGFR2 is a critical regulator of angiogenesis and is targeted for therapeutic intervention in many diseases such as cancer (6, 7), yet its regulation is not fully understood. One VEGFR2 inhibitor is axitinib which is in late-stage oncology clinical trials (phase I to III) (8, 9). VEGFR2 is a type III receptor tyrosine kinase in the PDGFR family with PDGFR α/β , c-Kit, FLT3, and CSF-1 (cFMS) as other members. The receptor is comprised of multiple domains that perform distinct biological functions: an extracel-

lular ligand binding domain with seven immunoglobulin-like motifs, a single transmembrane domain, a juxtamembrane domain (JM), a catalytic domain split by a kinase insert domain (KID), and a C-terminal docking domain (7, 10). VEGFR2 tyrosine residues are known to be phosphorylated in response to ligand stimulation (11, 12). Phosphorylation of tyrosine residues 1054 and 1059 in the activation loop has been shown to be essential for kinase activity (11, 13). Other regulatory mechanisms are more controversial. Cellular studies of the function of the murine VEGFR2 C-terminal docking domain tyrosine residue 1212 elucidated a role in the autophosphorylation reaction and kinase activation (14, 15). Similar studies with human VEGFR2 found the residue phosphorylation status to be dispensable to the activation process (12). Subsequent Y1212F VEGFR2 knock-in studies in mice showed that a phosphorylation of this residue was not necessary for *in vivo* function (16). Additionally, autophosphorylation of the two murine VEGFR2 JM tyrosine residues was reported to have no role in kinase activity or ligand-dependent activation through the analysis of phenylalanine mutants in cellular studies (14, 15, 17). From structural studies of related tyrosine kinases (e.g., insulin

*Correspondence should be addressed to this author. Tel: 858-622-6038. Fax: 858-526-4240. E-mail: brion.murray@pfizer.com.

¹Abbreviations: VEGFR-2, vascular endothelial growth factor receptor-2; VEGFR2-CD, VEGFR2 catalytic domain; VEGFR2-CD/JM, VEGFR2 catalytic domain/juxtamembrane domain; RTK, receptor tyrosine kinase; JM, juxtamembrane domain; CD, catalytic domain; KID, kinase insert domain; HEPES, *N*-(2-hydroxyethyl)piperazine-*N'*-2-ethanesulfonic acid; DTT, dithiothreitol; ATP, adenosine 5'-triphosphate; SDS–PAGE, sodium dodecyl sulfate–polyacrylamide gel electrophoresis; TCEP, tris(2-carboxyethyl)phosphine hydrochloride.

receptor), others have proposed a role for the VEGFR2 JM domain in the activation process (18). Detailed reports of enzymatic and structural characterization of VEGFR2 have thus far been confined to the catalytic domain (10, 19).

Regulation of RTKs has been shown to be governed by multiple phosphorylation events. Autophosphorylation of residues on the activation loop of the catalytic domain is one such well-characterized mechanism shown to regulate its catalytic activity (7, 20–22). An emerging understanding of the JM domain, which separates the catalytic domain from the transmembrane domain, reveals three possible regulatory mechanisms effected by JM autophosphorylation (18, 20, 23–28). One mechanism is that phosphorylation of JM tyrosine residue(s) creates binding sites for regulatory proteins. For the insulin receptor (IRK), autophosphorylation of the JM effects binding of regulatory proteins and does not alter catalysis (18, 25, 29). In a second mechanism, the JM domain adopts an α -helical structure in the unactivated kinase and binds to an autoinhibitory cleft in the N-terminal subunit of the catalytic domain which distorts the conformation of the catalytically important α C-helix (control helix). Eph receptors, MUSK, and TGF β receptors are regulated by this mechanism (18, 23, 29–32). In a third mechanism, the JM can bind in the interface between the N- and C-terminal subunits of the catalytic domain. This binding interaction sterically prevents the activation loop of the C-terminal subunit from adopting a catalytically productive conformation and also disrupts the N-terminal α C-helix. The type III receptor tyrosine kinases FLT3 (24), c-Kit (26, 27), and CSF-1 (cFMS) (28) have been shown crystallographically to utilize this binding mode. Enzymatic studies of c-Kit show that phosphorylation of the JM domain is required for activation (33) and is exploited in cancer (34). Thus, JM domains play varying roles in kinase biology.

In this study, the JM interactions with the catalytic domain of VEGFR2 were investigated by biochemical, biophysical, and structural methods. Evidence is presented that the first event is an intramolecular autophosphorylation of the JM domain followed by phosphorylation of the activation loop of the catalytic domain. In addition, the first detailed biochemical, biophysical, and structural studies of the advanced clinical candidate axitinib are presented. The enzymatic reaction catalyzed by the VEGFR2 construct containing both the catalytic and JM domains was inhibited by axitinib with substantially greater potency than was the construct containing only the catalytic domain. Thermodynamic and structural studies support a new role for the JM domain: a N-terminal/C-terminal clasp that affects conformational equilibrium. These studies expose the limitations of using the isolated catalytic domain of VEGFR2 to recapitulate the appropriate active site topography, and the findings may be extended to other related kinases.

MATERIALS AND METHODS

Materials. Human minigastrin (LEEEEEAYGWMDf) was purchased from Bachem (Torrance, CA). The following reagents were purchased from Sigma Chemical Co. (St. Louis, MO): poly (Glu₄Tyr), gastrin, lactate dehydrogenase, pyruvate kinase, phosphoenolpyruvate, HEPES (*N*-(2-hydroxyethyl)piperazine-*N'*-2-ethanesulfonic acid), dithiothreitol, MgCl₂, ATP, TCEP, and NADH. A peptide designed to encompass VEGFR2 residues 786–805 was synthesized and purified to 98% purity (CPC Scientific, San Jose, CA). Compounds were synthesized as

described in patents: AG-13736 (35), AG-13974 (36), AG-28038 (35), and AG-28047 (37).

Expression and Purification of VEGFR2 Proteins. Two codon optimized (Geneart, Regensburg, Germany) human VEGFR2 genes comprising the catalytic and juxtamembrane domains (residues 786–1171, VEGFR2-CD/JM) and the catalytic domain (residues 806–1171, VEGFR2-CD) without the kinase insert domain deletions (residues 940–989) containing one point mutation (E990V) were cloned into pFastBac vectors. The VEGFR2-CD construct has previously been published (10, 19). Proteins were expressed in *Sf9* cells using 10 L Wave BioReactors with ESF-921 protein-free media (Expression Systems Woodland, CA). Cells were harvested after 48 h postinfection. The recombinant VEGFR2-CD/JM protein contained an N-terminal His₆ tag followed by an HRV3C protease cleavage site. The VEGFR2 catalytic domain contained a C-terminal His₆ tag with an upstream TEV protease site. Clarified cell lysate was passed over a 10 mL Probond nickel column (Invitrogen, Carlsbad, CA). Tag removal was carried out by incubation with the appropriate protease in concert with overnight dialysis. The untagged VEGFR2 proteins were separated from proteases, free His₆ tag, and uncleaved protein by a second nickel chromatography step. Nontagged proteins were concentrated and loaded to a HiLoad 26/60 Superdex-75 column (GE Healthcare Tampa, FL) equilibrated in 50 mM HEPES, pH 7.5, + 30 mM NaCl + 5 mM DTT. Pooled fractions from the gel filtration column were concentrated to 8–13 mg/mL, flash-frozen in liquid nitrogen, and stored at –80 °C.

Enzymatic Assays. A spectrophotometric coupled enzymatic assay format was used to measure kinase activity. The kinase-catalyzed production of ADP from ATP that accompanies phosphoryl transfer to the random copolymer poly(Glu₄Tyr) was coupled to the oxidation of NADH through the activities of pyruvate kinase (PK) and lactate dehydrogenase (LDH). NADH conversion to NAD⁺ was monitored by the decrease in absorbance at 340 nm ($\epsilon = 6220 \text{ cm}^{-1} \text{ M}^{-1}$) using a Beckman DU650 spectrophotometer at 37 °C. Typical reaction solutions contained 2 mM phosphoenolpyruvate, 0.33 mM NADH, 50 mM MgCl₂, 5 mM DTT, ATP, minigastrin, or poly(Glu₄Tyr), 15 units/mL PK, and 15 units/mL LDH in 200 mM HEPES, pH 7.5. To determine kinetic parameters, ATP was varied from 7.8 to 8000 μM , poly(Glu₄Tyr) was varied from 0.013 to 13.7 mg/mL, and minigastrin was varied from 8.3 to 2150 μM . To calculate the concentration of available tyrosine residues in a given amount of poly(Glu₄Tyr), the minimum unit that contains tyrosine (Glu₄Tyr) was calculated to have a MW of 679.66. When poly(Glu₄Tyr) was used, assays were initiated with the addition of 10 nM nonphosphorylated VEGFR2-CD or VEGFR2-CD/JM; 5.0 nM nonphosphorylated VEGFR2-CD or VEGFR2-CD/JM was added when minigastrin was used as the phosphoacceptor. The same coupled enzymatic assay format was used for K_i determinations. The concentration of ATP was 10.8 mM; the concentration of poly(Glu₄Tyr) was 13.7 mg/mL. Inhibitor K_i determinations for nonphosphorylated VEGFR2-CD were initiated with the addition of 10 nM enzyme. Inhibitor K_i determinations for nonphosphorylated VEGFR2-CD/JM were initiated with the addition of 10.8 mM ATP, following a 10 min preincubation of enzyme and inhibitor at 37 °C in the reaction mix. K_i determinations were made from a plot of the fractional velocity as a function of inhibitor concentration fit to the Morrison equation with the enzyme concentration as a variable (38, 39).

Autophosphorylation of VEGFR2. Autophosphorylation reactions contained 5 mM ATP, 50 mM MgCl_2 , 5 mM DTT, 0.005% Tween-20, and 100 nM nonphosphorylated VEGFR2-CD or VEGFR2-CD/JM in 200 mM HEPES (pH 7.5) in a total volume of 9 mL. Reactions were initiated by the addition of 5 mM ATP and allowed to proceed at room temperature. Samples of 1200 μL were removed at 0, 2.5, 5, 10, and 30 min and stopped with 300 μL of 500 mM EDTA. Samples were concentrated at 4 °C to 10 μL using Nanosep 10K Omega filter membranes (Pall Life Sciences, Ann Arbor MI), and evaluated by isoelectric (IEF) chromatography. Concentrated samples were mixed with 10 μL of 2 \times IEF 3-10 sample buffer (Invitrogen, Carlsbad, CA). Standards were IEF 3-10 liquid mix (Serva Electrophoresis, Heidelberg, Germany). Samples and standards were loaded into an XCell mini-Cell containing a 3-10 IEF gel with 3-10 cathode and anode buffer (Invitrogen, Carlsbad, CA). Chromatography conditions were as follows: 100 V constant for 1.0 h, 200 V constant for 1.0 h, and 500 V constant for 30 min. The gels were fixed with 12% trichloroacetic acid containing 3.5% sulfosalicylic acid for 30 min and stained with Bio-Rad Coomassie Brilliant Blue 250 (Hercules, CA).

The autophosphorylation rate was measured as a function of VEGFR2-CD/JM concentration. Reactions contained 200 μM ATP (400 nCi/nmol), 50 mM MgCl_2 , and 3 mM DTT in 200 mM HEPES (pH 7.5). Reactions with varied enzyme concentrations (100, 250, 500, and 1000 nM) were initiated by the addition of 5 μg of VEGFR2-CD/JM and allowed to proceed at room temperature. They were stopped by the addition of a 4-fold excess of EDTA after 5 min. Samples were concentrated at 4 °C to 20 μL using Nanosep 10K Omega filter membranes (Pall Life Sciences, Ann Arbor, MI). Samples were analyzed by IEF gel (as above) and SDS-PAGE chromatography with both Coomassie stain and autoradiographic imaging. SDS-PAGE concentrated samples (10 μL) were mixed with 5 μL of 4 \times LDS sample buffer and 2 μL of 10 \times reducing agent (Invitrogen, Carlsbad, CA), and 3 μL of water. The samples were heated to 70 °C for 10 min. Standards were SeeBlue Plus 2 prestained standards (Invitrogen, Carlsbad, CA). Samples and standards were loaded into an XCell mini-Cell containing a NuPAGE Bis-Tris mini gel with 1 \times SDS running buffer (Invitrogen, Carlsbad, CA). The gel was run at 200 V constant for 45 min and stained with Bio-Rad Coomassie Brilliant Blue 250 (Hercules, CA).

Mass Spectrometric Analysis of the Autophosphorylation Reaction. Conditions were initially set to allow for large extents of reaction. Reaction solutions contained ATP, 50 mM MgCl_2 , 5 mM DTT, 0.005% TW-20, and 40 μM nonphosphorylated VEGFR2-CD or VEGFR2-CD/JM in 200 mM HEPES (pH 7.5) with a total volume of 100 μL . The autophosphorylation reactions were initiated by the addition of ATP, which was varied at 0, 0.1, 1.0, and 10 mM, and allowed to continue at room temperature for 3 min before being stopped by the addition of 25 μL of 500 mM EDTA. In a second set of experiments, the reaction conditions were modified to resolve the earlier phosphorylation events. These samples were prepared identically to the autophosphorylation IEF time courses with the exception of the time points taken. Samples were removed at 0, 0.5, 1, 2, 5, 10, and 30 min.

(A) Intact Protein Analysis by LC/MS. All intact analyses were performed on a Waters Micromass (Milford, MA) LCT time-of-flight mass spectrometer equipped with an electrospray ionization source interfaced to an Agilent (Santa Clara, CA) 1100 HPLC and run in positive ion mode. The

VEGFR2-CD and VEGFR2-CD/JM samples were diluted to 100 $\mu\text{g}/\text{mL}$ in 0.1% formic acid (JT Baker, Phillipsburg, NJ). A total of 2 μg (20 μL) of each autophosphorylated protein was injected using a PAL-HTS autosampler (LEAP Technologies, Carrboro, NC) and loaded onto a heated (60 °C) Micro Protein trap column (1 \times 10 mm; Michrom Bioresources, Auburn, CA) for desalting with 5% acetonitrile (ACN; Burdick & Jackson, Muskegon, MI) and 0.1% FA. The proteins were eluted with a 2 min gradient of 5–95% ACN (0.1% FA) at a flow rate of 0.5 mL/min for MS detection.

(B) Proteolysis. For every time point, a total of 1 μg of the VEGFR2-CD and VEGFR2-CD/JM proteins was digested separately with 40 μL of Promega sequencing grade trypsin (Madison, WI) and 40 μL of Roche chymotrypsin (Penzberg, Germany). The protease powders were dissolved in 50 mM aqueous ammonium bicarbonate (pH = 7.8) (Sigma Aldrich, St. Louis, MO) to the following concentrations: 20 $\mu\text{g}/\text{mL}$ trypsin and 50 $\mu\text{g}/\text{mL}$ chymotrypsin. Enzymatic digestion of the non-reduced proteins proceeded to completion using a 1.1 ft³ microwave oven (Magic Chef, Benton Harbor, MI) at 80% power for a total of 10.5 min. The enzymatic reactions were each quenched with 10 μL of 10% ACN with 5% FA.

(C) LC/MS/MS. Peptides were sequenced by LC/MS/MS using a ThermoFinnigan (San Jose, CA) LTQ linear ion trap mass spectrometer with a Michrom Bioresources ADVANCE Plug and Play Nano Spray source interfaced to an Eksigent (Dublin, CA) NanoLC 2D system. For each analysis, 100 ng of peptides was injected and loaded onto a Waters Atlantis dC18 NanoEase column (5 μm) for sample cleanup with 2% ACN and 0.1% FA. The peptides were subsequently eluted from the NanoEase column and loaded on a Phenomenex (Torrance, CA) Onyx Monolithic C18 nanoLC column (0.1 \times 150 mm) and eluted with a 53 min gradient of 2–45% ACN (0.1% FA) at a flow rate of 1 $\mu\text{L}/\text{min}$ for MS detection. Each full scan was followed by six alternating data-dependent zoom and MS/MS scans. The MS/MS data were searched against a targeted database using Agilent Spectrum Mill software.

Isothermal Titration Calorimetry (ITC). ITC experiments were carried out on a VP ITC instrument (GE Healthcare) at 30 °C. The VEGFR2 proteins were exchanged into a buffer containing 150 mM NaCl, 25 mM HEPES, pH 8.0, 5.0 mM MgCl_2 , 5% (v/v) glycerol, and 0.5 mM TCEP using a Superdex-75 size exclusion column (GE Healthcare), and the concentration was determined spectrophotometrically with a 340–220 nm scan using an ϵ_{280} of 45380 $\text{M}^{-1} \text{cm}^{-1}$. Compounds were diluted from 100% DMSO stocks into a buffer without DMSO. In a typical experiment, nineteen 15 μL injections of 150 μM compound were made into a 20 μM VEGFR2 solution. Heats of dilution were determined in a separate experiment. For the displacement binding studies, the high-affinity ligand was titrated into the protein solution pre-equilibrated with the low-affinity ligand at a concentration of 100 μM . Data from the direct binding experiments were analyzed using the ORIGIN software provided with the instrument and fit to a simple 1:1 binding model as described by Wiseman (40). For the displacement experiments data were analyzed as described by Sigurskjold (41) using the ORIGIN software. Errors were calculated based on data from experiments carried out in duplicate.

Surface Plasmon Resonance (SPR) Binding Studies. SPR binding studies were carried out using a Biacore 3000 instrument (GE Healthcare) at 25 °C in a 150 mM NaCl, 25 mM HEPES, pH 8.0, 5 mM MgCl_2 , 0.005% P20 surfactant

(GE Healthcare), and 0.5 mM DTT buffer. The VEGFR2-CD/JM protein was immobilized on a Biacore CM5 chip (GE Healthcare) by standard EDC/NHS amine coupling chemistry at 25 °C using a 1 μ M solution of the protein in 10 mM sodium acetate, pH 5.5. In a typical experiment 180 μ L injections were made using the Kinject injection mode at a flow rate of 50 μ L/min and a dissociation time of 2800 s. Data analysis was performed using the Scrubber2 software (BioLogic Software, Pty., Australia). Compound injections were referenced to a blank surface and by a buffer blank. Kinetic characteristics were obtained from a fit to a kinetic binding model (42) with mass transport using the Scrubber2 program.

Differential Scanning Calorimetry (DSC). DSC scans were collected on a MicroCal VP DSC instrument. Protein samples were exchanged into 25 mM HEPES, pH 8.0, 5 mM MgCl₂, 150 mM NaCl, 5% (v/v) glycerol, and 0.5 mM (TCEP), and the concentration was determined using the method described in the ITC section prior to the experiment. Scans were run from 20 to 90 °C using a rate of 90° per hour and a protein concentration of 12 μ M. Repeat scans showed that none of the protein tested unfolded reversibly under the conditions used. An average of three repeat scans was used to calculate an observed melting temperature (T_m) using the ORIGIN software provided with the instrument.

VEGF-Induced HUVEC Cellular Survival Assay. HUVEC cells (Clonetics) at passage five were plated in 100 μ L of F12K growth medium at a concentration of 1×10^4 cells per well in a 96-well plate and allowed to attach overnight. Cells are then starved in 1% FBS F12K media for 24 h. After starvation, 15 μ L of compounds formulated in 1% DMSO starvation media was added in triplicate to obtain a dose response curve (1:3 dilution). One hour after compound treatment, cells are stimulated with rhVEGF (R&D systems) at a final concentration of 20 ng/mL. After 72 h of incubation HUVEC cell survival was measured via an MTT assay (Promega). Absorption was measured at 570 nm with a 630 nm background subtraction. IC₅₀ values were calculated using negative (no rhVEGF, no compound) and positive (rhVEGF, no compound) controls as 0% and 100% survival, respectively.

RESULTS

Enzymatic Characterization of VEGFR2-CD and VEGFR2-CD/JM Substrate Processing. Since a prerequisite

for mechanistic studies is highly purified enzyme, methods were developed to isolate highly pure and active preparations of both nonphosphorylated VEGFR2-CD (10) and the nonphosphorylated VEGFR2-CD/JM. Neither constructs are full length and are missing the extracellular, transmembrane, and carboxy-terminal domains. All studied proteins were purified to homogeneity as evidenced by a single band on a SDS-PAGE gel with an estimated purity >95% (data not shown). The intact mass determinations corresponded to the expected calculated masses. For example, the VEGFR2-CD/JM construct has an expected mass of 38343 Da, and the measured mass was determined to be 38339 Da. By active site titration (43) with axitinib, all constructs had >90% of the active sites competent to bind the specific VEGFR2 inhibitor axitinib (data not shown). The kinetic parameters (Table 1) demonstrate that the VEGFR2 preparations are as active as or more active than previously reported (13, 19), which further indicates that there is an appropriate level of purity. To assess whether the autophosphorylation reaction is intra- or intermolecular, the monomer/dimer state of the proteins must be known. Analytic size exclusion chromatography evaluation (Phenomenex S3000 column) of the VEGFR2-CD/JM (339 μ M) is consistent with VEGFR2-CD/JM purified as a monomer (Figure 1). To more precisely evaluate the multimer state of the proteins, an additional analytical size exclusion chromatography column was used that was more sensitive in the range of expected molecular masses. Both proteins (200 μ M) were run on a calibrated Superdex-75 column. Based on the protein standards, the VEGFR2-CD eluted as a 46.9 ± 0.3 kDa protein while the VEGFR2-CD/JM protein eluted as a 43.8 ± 0.7 kDa protein. Since size exclusion chromatography is sensitive to both size and shape, the observation that the smaller protein eluted as a larger protein may be a function of the shape. This finding was also observed when the Phenomenex S3000 analytic SEC column was used (data not shown). The calorimetry studies (see below) show that the VEGFR2-CD/JM protein has a higher T_m , which may reflect a more compact structure. Even when tested at very high concentrations, both chromatographic analyses are consistent with the proteins present as monomers.

The kinetic parameters of the VEGFR2 catalytic domain with and without the full JM domain were determined with four different phosphoacceptor substrates. A peptide encompassing the extra residues included in the VEGFR2-CD/JM construct (VEGFR2 residues 786–805) was evaluated as a potential substrate because it contained a tyrosine residue (Y801). At

Table 1: Kinetic Parameters for VEGFR2-CD and VEGFR2-CD/JM Proteins^a

		ATP	poly(Glu ₄ Tyr)	minigastrin	gastrin
VEGFR2-CD nonphosphorylated	K_m (mM)	0.776 ± 0.025	3.99 ± 0.227	0.893 ± 0.012	0.311 ± 0.012
	k_{cat} (s ⁻¹)	27.5 ± 0.28	25.9 ± 0.536	43.1 ± 0.941	36.1 ± 0.72
	k_{cat}/K_m (M ⁻¹ s ⁻¹)	35400 ± 1170	6670 ± 379	48200 ± 1050	116000 ± 4180
VEGFR2-CD/JM nonphosphorylated	K_m (mM)	2.00 ± 0.150	3.60 ± 0.206	0.634 ± 0.014	0.266 ± 0.012
	k_{cat} (s ⁻¹)	23.0 ± 0.434	23.7 ± 0.587	29.0 ± 0.267	27.6 ± 0.552
	k_{cat}/K_m (M ⁻¹ s ⁻¹)	11500 ± 863	6580 ± 376	45800 ± 1010	104000 ± 3740
VEGFR2-CD fully phosphorylated	K_m (mM)	0.176 ± 0.006	2.7 ± 0.358	ND	ND
	k_{cat} (s ⁻¹)	18.7 ± 0.14	24.3 ± 0.91	ND	ND
	k_{cat}/K_m (M ⁻¹ s ⁻¹)	106000 ± 3610	9000 ± 288	ND	ND
VEGFR2-CD/JM fully phosphorylated	K_m (mM)	0.14 ± 0.010	3.6 ± 0.206	ND	ND
	k_{cat} (s ⁻¹)	12 ± 0.22	23.7 ± 1.35	ND	ND
	k_{cat}/K_m (M ⁻¹ s ⁻¹)	86000 ± 6100	6580 ± 376	ND	ND

^a 10 mM ATP was used for all K_m phosphoacceptor determinations. The K_m for ATP was determined with 20 mM poly(Glu₄Tyr). Both constructs have similar substrate processing values with the exception of ATP, which is 3-fold lower for nonphosphorylated VEGFR2-CD/JM.

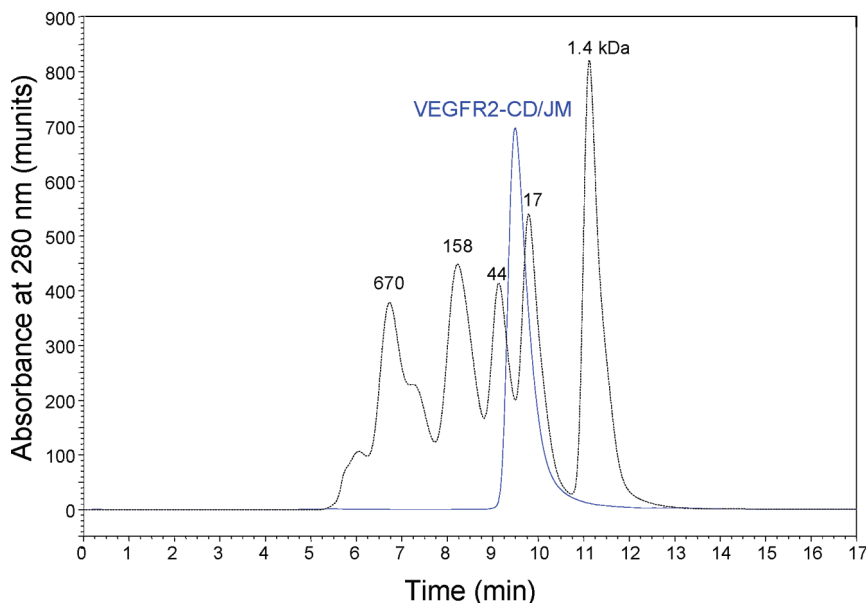


FIGURE 1: VEGFR2-CD/JM is purified as a monomer. VEGFR2-CD/JM (0.15 mg, 13 mg/mL) was injected into a S3000 analytical gel filtration column (Phenomenex) (—). The S3000 column was calibrated (---) with protein standards: thyroglobulin (670 kDa), IgG (158 kDa), ovalbumin (44 kDa), myoglobin (17 kDa), and vitamin B₁₂ (1.4 kDa).

peptide concentrations as high as 2.5 mM, there was minimal to no detectable phosphorylation of this peptide by either VEGFR2-CD or VEGFR2-CD/JM constructs. Both fully activated constructs had similar kinetic parameters with all three general tyrosine kinase substrates (Table 1). The catalytic efficiency (k_{cat}/K_m) for both nonphosphorylated VEGFR2-CD and nonphosphorylated VEGFR2-CD/JM constructs is similar for three substrates tested (Table 1). The only significant difference was found for the $K_{m,\text{ATP}}$ value, which was 3-fold higher for nonphosphorylated VEGFR2-CD/JM compared to nonphosphorylated VEGFR2-CD. For the nonphosphorylated VEGFR2-CD construct, there is no expected change in the autophosphorylation state in the time that kinetic measurements were taken. In contrast, the VEGFR2-CD/JM protein has a rapid autophosphorylation reaction on a tyrosine residue in the JM domain (Figure 2) which may lead to the formation of a population of singly phosphorylated VEGFR2-CD/JM protein at high ATP concentrations in the time scale of the analysis. For VEGFR2-CD/JM, the production of ADP was determined to be linear for 10 min of reaction, which indicated that there was no large change in catalytic properties during the assay reaction time. The evaluation of VEGFR2-CD/JM was performed in a continuous assay format that allowed for the kinetic parameters to be measured as a function of time. There was no significant change in catalytic parameters determined with short time points (0–2 min) relative to longer time points (2–8 min). As such, either there was not a significant contribution of the phosphorylated form of VEGFR2-CD/JM to the nonphosphorylated data or the phosphorylation of Y801 does not have a significant impact on catalytic parameters. Nonetheless, data from all of the evaluated substrates show that both constructs have similar catalytic properties.

Autophosphorylation Reaction. The time courses of the VEGFR2-CD/JM and VEGFR2-CD autophosphorylation reactions were investigated to identify any overt differences in the reaction rates. Autophosphorylation reactions for both constructs were monitored at high ATP concentrations (5 mM) and low enzyme concentrations (100 nM) with the extent of the

reactions monitored by Coomassie-stained isoelectric focusing gel electrophoresis (IEF): VEGFR2-CD/JM (Figure 2A) and VEGFR2-CD (Figure 2B). Mobility in an IEF gel is affected by charge (e.g., phosphorylation state) and shape (conformation). IEF analysis revealed that nonphosphorylated VEGFR2-CD/JM is predominantly a single species with a major band at $pI = 7.8$. In the first 2.5 min of reaction, most of the nonphosphorylated species had shifted to a second species with a major band of $pI = 7.5$. Minor bands were observed (e.g., $pI = 7.7$ and 7.4) and may represent a small fraction of the preparation present in an alternative conformation (e.g., JM bound to the CD vs JM tethered to the CD). Additional phosphorylation events became apparent after 5 min of reaction (Figure 2A). After 30 min of reaction time, the nonphosphorylated species is not present, and there is one dominant species at $pI = 7.5$ with minor bands ranging in pI values from 7.4 to 6.2 (see Figure 2A). In contrast, for the 30 min reaction, there was almost no detectable VEGFR2-CD autophosphorylation with only one major band with $pI = 6.5$ (Figure 2B). A minor band is faintly observed at 30 min ($pI = 6.5$) but is not visible in Figure 2B. An autophosphorylation event for VEGFR2-CD/JM occurs at a faster rate than any observed for VEGFR2-CD. A second phosphorylation event in the VEGFR2-CD/JM autophosphorylation reaction may occur at an enhanced rate relative to the first VEGFR2-CD autophosphorylation event (Figure 2B).

The identity of the rapid VEGFR2-CD/JM autophosphorylation event may be important to understand the molecular underpinning of VEGFR2 biology. The autophosphorylation reaction of VEGFR2-CD/JM (100 nM) was measured at saturating ATP concentration (5 mM) and sampled over a 30 min room temperature time course (0, 0.5, 1, 2, 5, 10, 30 min). The extent of each reaction was monitored by ion trap mass spectrometry. As observed in the IEF analysis, the first phosphorylation event was detected after 30 s of reaction and increased in intensity over 30 min of reaction (Figure 2C). The second phosphorylation event was detected at low abundance for the first 10 min of the reaction and increased in abundance after 10–30 min. Samples from all of the time points of the time course were proteolyzed

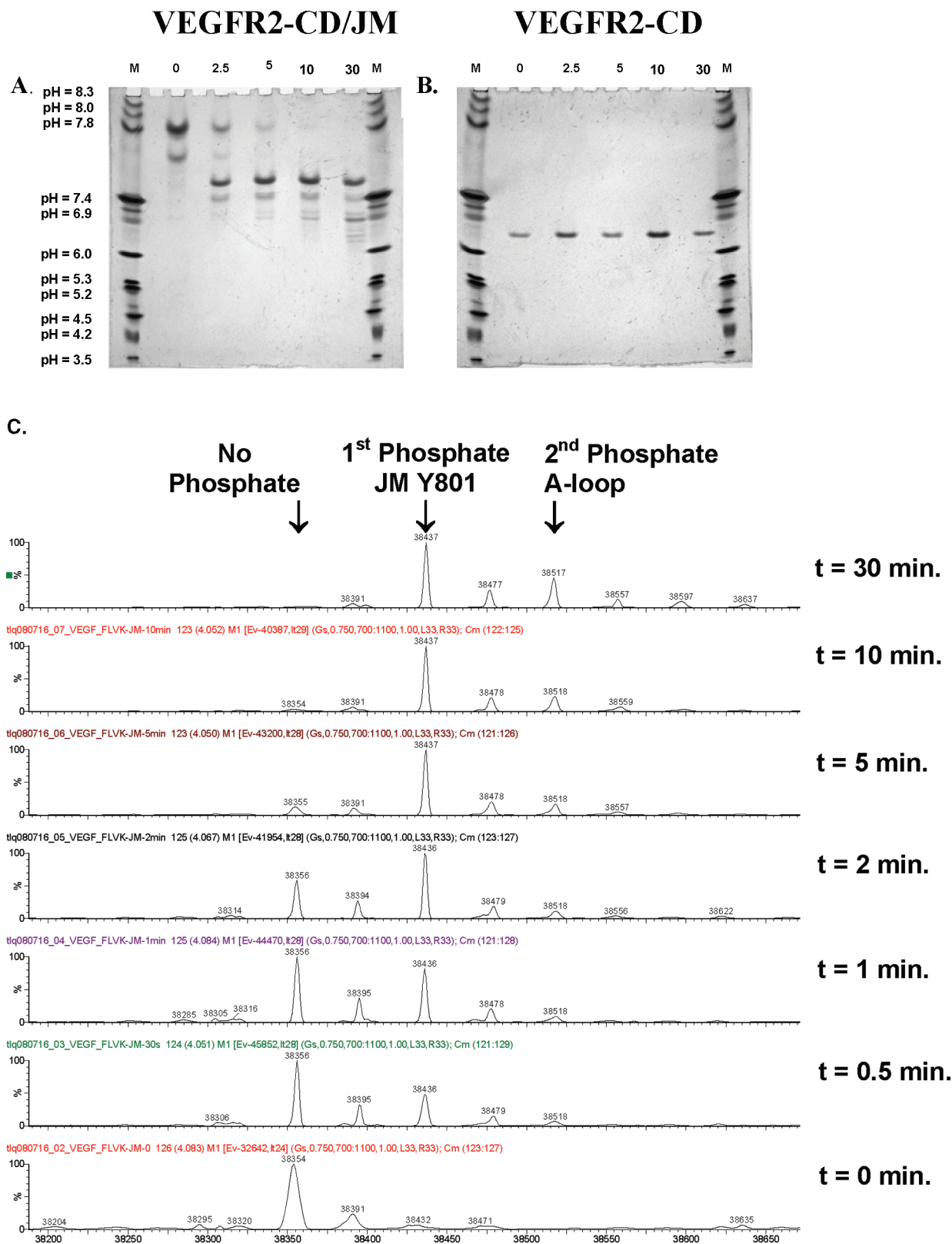


FIGURE 2: (A, B) IEF gel analysis of the autophosphorylation of VEGFR2-CD/JM (A) and VEGFR2-CD (B). IEF gels are run under nonreducing conditions such that different conformations of a single protein may be resolved to separate bands. Reaction mixtures contained 5 mM ATP, 50 mM MgCl₂, 5 mM DTT, 0.005% TW-20, and 100 nM VEGFR2-CD or VEGFR2-CD/JM in 200 mM HEPES (pH 7.5) in a total volume of 9 mL. Reactions were initiated by the addition of 5 mM ATP and allowed to proceed at room temperature. Samples (1.2 mL) were removed at 0, 2.5, 5, 10, and 30 min and stopped with the addition of 0.3 mL of a 500 mM EDTA solution. (C) Mass spectrometric analysis of the autophosphorylation reaction. Reactions were run at 100 nM VEGFR2-CD/JM, 5 mM ATP, and room temperature. Samples were removed at 0, 0.5, 1, 2, 5, 10, and 30 min. The extent of the reactions was monitored by ion trap mass spectrometry. The mass determinations were as follows: 38355 Da (no phosphate), 38437 Da (1 phosphate), and 38518 Da (2 phosphates). These same samples were proteolyzed with chymotrypsin and subjected to MALDI-TOF mass spectrometry to identify sites of phosphorylation.

with chymotrypsin and analyzed by MALDI-TOF mass spectrometry. The observed peptide coverage for samples at all time points ranged from 70% to 83%. The first phosphorylation site was identified to be tyrosine residue 801 in the JM domain and was the only observed phosphorylated residue in the 0.5–5 min samples. In the 10–30 min samples, phosphorylation of the activation loop residues Y1054 and Y1059 were observed.

The effect of VEGFR2-CD/JM concentration on the autophosphorylation rate of Y801 was studied to provide insight on whether the autophosphorylation event occurs by either an intermolecular or intramolecular mechanism. To allow for the selective phosphorylation of Y801, the reaction time was kept short (5 min) and the ATP concentration was low (0.2 mM). [32 P] Phosphate incorporation into the VEGFR2-CD/JM protein from [γ - 32 P]ATP was monitored at different enzyme concentrations (100, 250, 500, 1000 nM). IEF analysis was used to characterize the extent of reaction to ensure that only Y801 of the JM domain was phosphorylated while the SDS-PAGE format was used to accurately quantitate the relative amount of phosphate incorporation. IEF analysis showed the same pattern of bands for the different enzyme concentrations (data not shown). The resulting SDS-PAGE gel was quantified by autoradiography (Figure 3). To ensure that the signal did not exceed the dynamic range of autoradiography, quantitation with a phosphoimager was performed. The observations were reproduced in a subsequent experiment. Densitometry of the Coomassie-stained bands was used to normalize the amount of protein loaded into each well. There was no observed change in autophosphorylation rate of Y801 as a function of VEGFR2-CD/JM concentration (Figure 3).

Effect of the JM Domain on the Thermal Stability of the VEGFR2. To investigate the effect of the JM domain on the thermal unfolding of the VEGFR2 proteins, DSC experiments were carried out (Figure 4). Repeat scans on the protein showed an irreversible transition under the experimental conditions. This prevented a detailed thermodynamic analysis of the data to determine the ΔH and ΔC_p of unfolding. However, a unfolding temperature (T_m) was determined, which provides a relative measure of the folding stability of the protein. Since the unfolding was irreversible, care was taken to carry out experiments in triplicate, under the same concentration and scan rate, for each protein. The VEGFR2-CD was found to unfold with a T_m of 47.9 ± 0.15 °C. The VEGFR2-CD/JM construct exhibited an increase in T_m of approximately 2° to 49.7 ± 0.12 °C. A further small but significant increase in T_m was determined for the phosphorylated VEGFR2-CD/JM protein, which had an observed T_m of 50.7 ± 0.10 °C. This is consistent with a significant stabilization of the VEGFR2-CD/JM relative to the VEGFR2-CD.

Evaluation of Specific VEGFR2 Inhibitors. Inhibitors can be used as sensitive molecular probes of the topography of the active site, but care must be taken to determine accurate potency values. All inhibitors used in this study are noncovalent, ATP-competitive VEGFR2 inhibitors. The compounds were based on an indazole core with identical substituents at the 6-position and different substituents at the 3-position. The K_i values determined in this study were low relative to the total enzyme concentration (5–10 nM). To maximize the sensitivity of the enzymatic assay, a high level of ATP (10.8 mM) was used to drive the free VEGFR2 protein concentration to 0.7 nM: $[E \cdot S]/[E] = [S]/([S] + K_m)$. Using tight-binding kinetics, it has been shown that a properly designed study can determine K_i values that are of a magnitude of 1% of the enzyme concentration (39). In addition, to achieve very

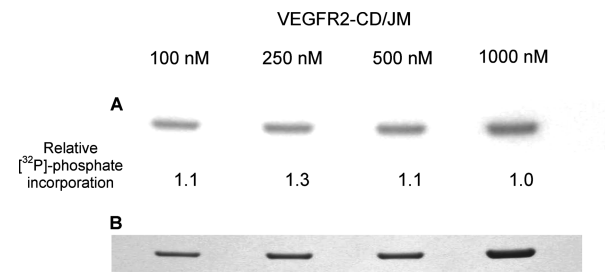


FIGURE 3: Autophosphorylation of VEGFR2-CD/JM tyrosine residue 801 as a function of enzyme concentration. The relationship between VEGFR2-CD/JM concentration and autophosphorylation. (A) Autoradiogram and (B) Coomassie Brilliant Blue 250 stain of SDS-PAGE gel. There is a 1 to 1 correspondence between the amount of protein loaded and the amount of 32 P incorporation across all VEGFR2-CD/JM concentrations.

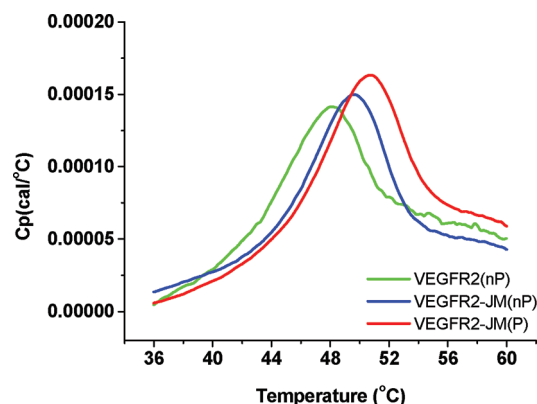
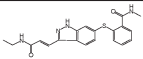
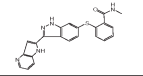
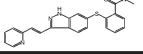


FIGURE 4: DSC thermal stability analysis of VEGFR2-CD and VEGFR2-CD/JM. DSC data show the effect of the JM domain and phosphorylation on the observed thermal unfolding characteristics of the VEGFR2 protein. Data shown are for the average of three separate scans of 12 μ M VEGFR2 proteins. A T_m of 47.9 ± 0.15 °C was observed for the VEGFR2-CD protein compared to 49.7 ± 0.12 and 50.7 ± 0.10 °C for the VEGFR2-CD/JM and phosphorylated VEGFR2-CD/JM protein, respectively.

accurate potency values, data points needed to be carefully selected (39). Since the autophosphorylation reaction of VEGFR2-CD is not fast on the time scale of the biochemical assay, conditions can be set so activity of either nonphosphorylated or fully autophosphorylated VEGFR2-CD can be measured (Figure 2B). Axitinib was determined to be a potent inhibitor of the nonphosphorylated VEGFR2-CD protein ($K_i = 1.10 \pm 0.06$ nM) with reduced inhibitory potency toward the phosphorylated form, which is consistent with an inhibitor that binds to a “DFG-out” conformation. Axitinib potency toward nonphosphorylated VEGFR2-CD with multiple phospho acceptors was investigated to determine if the potency was dependent on the phosphoacceptor. With poly(Glu₄Tyr) (Table 2), activation loop peptide KDR ($K_i = 0.88 \pm 0.23$ nM), and the activation loop peptide of the kinase c-Met ($K_i = 0.69 \pm 0.12$ nM, Met2 peptide), the axitinib inhibitory potency was found to be invariant. Axitinib was evaluated with an additional construct that contained the entire catalytic domain including the kinase insert domain, and the determined potency ($K_i = 0.75 \pm 0.12$ nM, Met2 peptide) was equivalent to values derived with the VEGFR2-CD. Next, the effect of VEGFR2 phosphorylation state on inhibitor potency was evaluated. When the inhibition of fully phosphorylated VEGFR2-CD protein was evaluated, a 7-fold increase in K_i value for axitinib was observed compared to

Table 2: Effect of the JM Domain on Inhibition of Catalytic Domain Enzymatic Activity^a

Compound	Structure	Nonphosphorylated		Phosphorylated		Cellular
		VEGFR2-CD	VEGFR2-CD/JM	VEGFR2-CD	VEGFR2-CD/JM	HUVEC
		K_i (pM)	K_i (pM)	K_i (pM)	K_i (pM)	IC_{50} (pM)
AG-28038		19000±250	630±62	53250±4200	30600±4200	6600
AG-28047		1100±20	50±4.3	5572±440	2000±240	400
Axitinib		1100±55	28±3.5	7200±900	1220±130	300

^a K_i values were determined in biochemical assays and the HUVEC IC_{50} value survival assay of VEGF-stimulated HUVEC cells.

nonphosphorylated VEGFR2-CD (Table 2). Other related inhibitors were also shown to be more potent for the nonphosphorylated VEGFR2-CD (Table 2). Next, studies were performed to evaluate the effect of the JM domain on inhibition of the nonphosphorylated VEGFR2 catalytic domain. Measuring inhibition of nonphosphorylated VEGFR2-CD/JM was difficult due to the fast autophosphorylation reaction. Without a preincubation, the K_i of AG-013974 was determined to be 650 pM. Since the nonphosphorylated VEGFR2-CD/JM protein undergoes a rapid autophosphorylation reaction at high ATP concentrations, the potency value may encompass inhibition of multiple phosphorylation states of VEGFR2-CD/JM. To allow the inhibitors to bind to the fully nonphosphorylated form of VEGFR2-CD/JM, compounds were added in the absence of ATP. AG-013974 was preincubated with nonphosphorylated VEGFR2-CD/JM for variable times (0, 5, 15, 30, 60 min) in the absence of ATP to determine optimal preincubation time. With brief compound preincubation times (5–10 min) the K_i was 120 pM, a 5-fold shift. No further shift was seen for longer times. The data are consistent with enhanced potency toward the nonphosphorylated form of VEGFR2-CD/JM but cannot be used to rule out a modest time dependency to the acquisition of full inhibitory potency. Since the biochemical inhibitory potency was constant after 5 min of preincubation, a 10 min preincubation time was used for subsequent studies with the VEGFR2-CD/JM construct. After a 10 min preincubation of AG-28038 with the nonphosphorylated VEGFR2-CD/JM, a reproducible 4-fold enhancement of potency was observed to yield a final K_i value of 630 ± 62 pM (Table 2). The inhibition constant (K_i) of AG-28038 determined with the nonphosphorylated VEGFR2-CD was invariant upon inhibitor preincubation times up to 60 min. Since the autophosphorylation reaction is slower for VEGFR2-CD, there may be no need to “trap” the unphosphorylated form of VEGFR2-CD in an inhibitor–protein complex. When comparing the potency of AG-28038 between the two VEGFR2 proteins, AG-28038 was found to be a 30-fold more potent inhibitor of the nonphosphorylated VEGFR2-CD/JM protein relative to nonphosphorylated VEGFR2-CD protein. Inhibitors AG-028047 and axitinib demonstrated greater potency (22-fold and 44-fold, respectively) for VEGFR2-CD/JM relative to VEGFR2-CD (Table 2). As was observed with VEGFR2-CD, phosphorylation of VEGFR2-CD/JM results in reduced inhibitor potency. The SAR with the nonphosphorylated JM domain tracked with the cellular potency found in Table 2 and has been observed for a

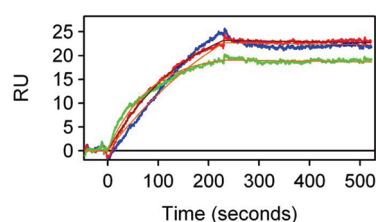


FIGURE 5: SPR real time kinetics of axitinib binding VEGFR2-CD/JM. SPR data for VEGFR2-JM at 25 °C: 2.5 nM (blue), 5 nM (red), and 10 nM (green) axitinib. The line shows the fit to a simple model with mass transport using the Scrubber2 program. The observed kinetic characteristics were as follows: axitinib $k_a = (1.4 \pm 0.2) \times 10^6 \text{ M}^{-1} \text{ s}^{-1}$, $k_d = 7.2 \times 10^{-5} \text{ s}^{-1}$, and $K_{D,obs} = 53 \pm 7 \text{ pM}$. Because the dissociation was very slow, the $K_{D,obs}$ for axitinib most likely represents an upper limit of the K_D .

wider array of compounds (unpublished results). As the axitinib K_i value was only 4% of the free VEGFR2-CD/JM concentration, we sought to find independent methods to validate the potency determination.

Compound Binding to the VEGFR2 Characterized by Surface Plasmon Resonance. The high observed biochemical potency for the inhibitors was expected to be corroborated by a slow rate of dissociation. To quantitate the dissociation rates of the inhibitors bound to VEGFR2-CD/JM, real time kinetic studies were carried out using surface plasmon resonance (SPR) biosensor technology (Figure 5). For axitinib, the dissociation rate observed was extremely slow. From a global analysis, axitinib was determined to have an association rate (k_a) of $(1.4 \pm 0.2) \times 10^6 \text{ M}^{-1} \text{ s}^{-1}$, an upper limit dissociation rate (k_d) of $(7.2 \pm 0.7) \times 10^{-5} \text{ s}^{-1}$, and an upper limit of the equilibrium dissociation constant ($K_{D,obs}$) of $53 \pm 7 \text{ pM}$. The slow dissociation rate of axitinib did not allow accurate analysis of the dissociation rate. Nonetheless, the observed K_d value is in the range of the determined K_i value. The axitinib k_a and k_d values are consistent with values reported using SPR for a similarly potent molecule, diethylstilbestrol, binding to the estrogen receptor (44). Based on the slow dissociation rate, the half-life of the inhibitor–protein complex was estimated to be on the time scale of several hours.

ITC Displacement Studies To Validate the Potency Shift Observed in the Biochemical Assay. Due to the high potency of the evaluated inhibitors, both biochemical and isothermal titration calorimetry (ITC) displacement assays were used to

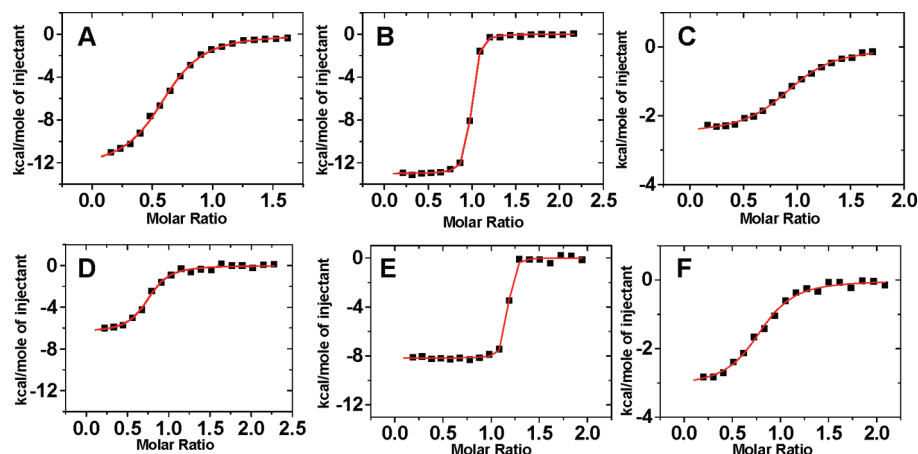


FIGURE 6: ITC displacement analysis to determine the effect of JM domain on the thermodynamics of compound binding. Isotherms show binding data for the VEGFR2-CD (A–C) and VEGFR2-CD/JM (D–F). The displacement experiment consists of two parts: first a weaker compound (PF-41316) is characterized (A and D). The affinity of the tight compound (AG-28038) is beyond the range of determination in the traditional mode of ITC (B and E), but in a second experiment the tight compound is measured in the presence of saturating amounts of the weak compound, and a competition binding isotherm is observed (C and F). Data were analyzed by an exact analysis method (41).

Table 3: Thermodynamic Binding Characteristics for PF-41316 and AG-28038 Binding to the VEGFR2-CD and VEGFR2-CD/JM Proteins^a

syringe	cell	$K_{B,obs}$ (M^{-1})	$K_{D,obs}$ (M)	ΔH_{obs} (kcal mol ⁻¹)	ΔG_{obs} (kcal mol ⁻¹)	$T\Delta S_{obs}$ (kcal mol ⁻¹)
PF-41316	VEGFR2-CD	$(2.4 \pm 0.5) \times 10^6$	$(0.43 \pm 0.08) \times 10^{-6}$	-11.2 ± 1.9	-8.8	-2.4
PF-41316	VEGFR2-CD/JM	$(7.3 \pm 3.5) \times 10^6$	$(0.15 \pm 0.07) \times 10^{-6}$	-7.5 ± 1.5	-9.5	+2.1
AG-28038	VEGFR2-CD + PF-41316	$(0.22 \pm 0.5) \times 10^9$	$(4.6 \pm 1.0) \times 10^{-9}$	-13.8 ± 1.6	-11.6	-2.2
AG-28038	VEGFR2-CD/JM + PF-41316	$(1.6 \pm 0.7) \times 10^9$	$(0.65 \pm 0.29) \times 10^{-9}$	-10.4 ± 1.3	-12.7	+2.3

^a AG-28038 binding was characterized by displacement experiments where the VEGFR2-CD protein was equilibrated with PF-41316 in the cell and titrated with AG-28038 from the syringe. The data were fit using an exact analysis method (41). $n = 0.82 \pm 0.14$ for all experiments.

characterize binding events. AG-28038 bound too tightly to directly determine a K_D for either nonphosphorylated construct by ITC (see Figure 6B,E). An ITC displacement method utilizing an ATP-competitive, modestly potent, small molecule ligand (PF-41316) was therefore used. PF-41316 was selected as an appropriate competitive ligand because it fulfilled the three essential criteria: (1) a K_D that could be accurately characterized in a separate experiment, (2) an observed ΔH sufficiently different from that of AG-28038, and (3) sufficient solubility that it could be equilibrated with the VEGFR2-CD at saturating concentrations for the displacement titration. The observed K_D values of PF-41316 for nonphosphorylated VEGFR2-CD and VEGFR2-CD/JM were 430 ± 80 and 150 ± 70 nM, respectively (Figure 6A,D). The displacement of PF-41316 by AG-28038 resulted in $K_{D,obs}$ values of 4.6 ± 1 and 0.65 ± 0.29 nM for nonphosphorylated VEGFR2-CD and VEGFR2-CD/JM, respectively (see Figure 6C,F). AG-28038 was 7-fold more potent toward VEGFR2-CD/JM than VEGFR2-CD ($\Delta\Delta G = 1.1$ kcal·mol⁻¹). These findings support the 30-fold shift in potency determined by kinetic measurements (Table 2). Similar displacement experiments were attempted for axitinib. However, this molecule was not sufficiently soluble at the concentration required for accurate measurement in the ITC experiment ($> 50 \mu M$).

Thermodynamic Characteristics of Binding to VEGFR2-CD and VEGFR2-CD/JM. ITC was used to determine the binding affinity of compounds to the VEGFR2-CD and VEGFR2-CD/JM proteins. In addition to binding affinity, ITC provides a direct measure of the observed binding enthalpy (ΔH_{obs}) which together with ΔG can be used to determine the observed entropy (ΔS_{obs}) change of binding. Evaluation of the

data reveals a trend in the thermodynamics of compounds PF-41316 and AG-28038 binding to the VEGFR2-CD and VEGFR2-CD/JM constructs (Table 3). The binding of both compounds to the VEGFR2-CD are characterized by large favorable ΔH and a smaller unfavorable ΔS contribution to the ΔG of binding ($\Delta H_{obs}(PF-41316) = -11.2 \pm 1.9$ kcal·mol⁻¹, $T\Delta S_{obs} = -2.4$ kcal·mol⁻¹; $\Delta H_{obs}(AG-28038) = -13.8 \pm 1.6$ kcal·mol⁻¹, $T\Delta S_{obs} = -2.2$ kcal·mol⁻¹). For the VEGFR2-CD/JM protein, the binding ΔG results from a slightly less favorable ΔH but now with a favorable ΔS_{obs} for binding of both compounds ($\Delta H_{obs}(PF-41316) = -7.5 \pm 1.5$ kcal·mol⁻¹, $T\Delta S_{obs} = 2.0$ kcal·mol⁻¹; $\Delta H_{obs}(AG-28038) = -10.4 \pm 1.3$ kcal·mol⁻¹, $T\Delta S = 2.3$ kcal·mol⁻¹). We were not able to characterize the thermodynamic profile of axitinib due to the insufficient solubility of the molecule.

DISCUSSION

Effect of the Protein Construct on VEGFR2 Catalysis. Autophosphorylation has been shown to have varied effects on RTK catalytic and functional properties. For example, autophosphorylation of the activation loop in the catalytic domain of Tie2 RTK has a profound effect on catalytic efficiency (460-fold increase in k_{cat}/K_m) (45) while with other RTKs such as EGF receptors there is no effect (20, 46). The JM domain has been shown to affect RTK catalysis (18). Receptor tyrosine kinases such as c-Kit utilize autophosphorylation to regulate the kinase activation rates but do not alter the maximal enzymatic activity (33). In contrast, the autophosphorylated insulin receptor JM residues serve only as docking sites for regulatory proteins (18, 29). Consistent with a previous finding for both the isolated VEGFR2 catalytic domain (19) or a GST fusion of a portion of

the VEGFR2 cytosolic domain (VEGFR2 residues 802–1356) (13), autophosphorylation did not have large effects on catalytic parameters for either the VEGFR2-CD or VEGFR2-CD/JM constructs.

Characterization of the VEGFR2 Autophosphorylation Reaction. The order of phosphorylation events in the autophosphorylation reaction can provide insight into RTK biology. The order of autophosphorylation events for the VEGFR2-CD/JM begins with the phosphorylation of tyrosine residue 801 in the JM domain and is followed by phosphorylation of tyrosine residues in the activation loop of the catalytic domain. Crystallographic studies of the insulin receptor (IR) revealed a significant role for a nonphosphorylated JM tyrosine residue analogous to VEGFR2 Y801 (IR Y984) which was predicted to extend to VEGFR2 (18). Unlike VEGFR2 Y801, the insulin receptor residue Y984 is not reported to be autophosphorylated (18, 25). Insulin receptor Y984 was shown to interact with conserved residues in the N-terminal subunit of the catalytic domain and stabilize a catalytically nonproductive conformation (25). The insulin receptor Y984 when mutated to a phenylalanine residue results in a 4-fold increase in basal activity but has no effect on the maximal activity achieved upon activation (25). Since the VEGFR2 catalytic domain with and without the JM domain has similar basal levels of catalytic activity, the JM domain does not appear to regulate the basal level of enzymatic activity. Furthermore, the corresponding VEGFR residue, Y801, was shown to be rapidly phosphorylated. Previous studies propose that phosphorylated VEGFR2 tyrosine residue 801 is a docking site for either phospholipase C- γ (47) or the p85 subunit of PI3K (14). Data presented here are consistent with a noncatalytic role for JM tyrosine residue 801.

The autophosphorylation of VEGFR2 JM domain residue Y801 is proposed to occur through an intramolecular autophosphorylation reaction which is supported by (1) the rapidity of the reaction, (2) the lack of phosphorylation of an exogenous 19 amino acid peptide, and (3) the invariance of the autophosphorylation reaction rate on the enzyme concentration. Intramolecular autophosphorylation reactions are rare but not without precedent. Both the leucine-rich repeat kinase-2 (LRRK2) (48) and interleukin-2 tyrosine kinase (Itk) (49) have been reported to perform an intramolecular autophosphorylation reaction. Itk phosphorylates the SH3 domain intramolecularly, and LRRK2 phosphorylates the catalytic domain activation loop. Nonetheless, intramolecular autophosphorylation of PDGFR family kinases is without precedent. Taken together, VEGFR2 appears to be rapidly autophosphorylated on a JM tyrosine residue by an intramolecular mechanism that does not significantly alter enzymatic properties.

Effect of the Kinase Construct on Inhibitor Potency. Biochemical assays are typically designed to mimic reactions as they occur in a cellular context as much as possible, yet routinely inhibitor potencies do not recapitulate potencies measured in cellular assays. There are many potential reasons for biochemical–cellular potency shifts: (a) in a cell, there is a high concentration of ATP, (b) the concentration of the inhibitor at the cellular target is different due to protein binding, permeability, efflux, and metabolism, (c) kinases can act in a time-dependent manner and have long residence times (50, 51) that synergizes with cellular regulatory mechanisms, and (d) the target in the cell is different. The current study evaluates the role of the protein construct on potency. The catalytic domain of kinases are routinely used to recapitulate the biochemical reactions of kinases

in inhibitor design (52). Biochemical inhibitor potencies determined with the VEGFR2-CD protein were weaker than the determined cellular IC_{50} and *in vivo* potency. Axitinib has been reported to potentially inhibit VEGFR2 autophosphorylation in cells: PAE cells (IC_{50} = 200 pM) and HUVEC cells (IC_{50} = 60 pM) (8). *In vivo*, axitinib inhibits VEGFR2 autophosphorylation with an IC_{50} = 490 pM (8). Considering that protein binding decreases the free fraction of inhibitor in the cellular and *in vivo* assays, the biochemical potency value derived from nonphosphorylated VEGFR2-CD/JM (K_i = 28 pM) is more consistent with the cellular potency data than nonphosphorylated VEGFR2-CD (K_i = 1100 pM). This may suggest that the VEGFR2 JM domain affects the inhibitor binding site and/or the conformational equilibria of the intracellular domain of VEGFR2 in cells. In addition, the studied inhibitors were potent toward the nonphosphorylated forms of the VEGFR2 proteins, which is consistent with an inhibitor that binds to the “DFG-out” catalytic domain conformation. These findings may extend to other RTK inhibitors. For example, both the PTK/ZK (53) and the YM-359445 (54) VEGFR2 inhibitors are more potent in cellular assays. The described findings reinforce the importance of selecting the proper protein construct to characterize inhibitor interactions.

Biophysical Evaluation of Inhibitor Binding Interactions to Both VEGFR2 Constructs. The accurate evaluation of the *in vitro* binding properties of highly potent small molecules represents a particular challenge to the capabilities of traditional biochemical and biophysical methods. To further evaluate the biochemical interactions of the VEGFR2 inhibitors, both surface plasmon resonance (SPR) and calorimetry approaches were used. The off-rate of axitinib was extremely slow, which complicated the SPR analysis. Nonetheless, the upper limit on the dissociation constant could be estimated by SPR (K_D \approx 50 pM), which is consistent with the inhibition constant derived from kinetic measurements (K_i = 28 pM). The high potency of VEGFR2 inhibitors exceeded the typical range of isothermal calorimetric (ITC) binding studies (double digit nanomolar range) where binding becomes stoichiometric in nature (40). A method for the exact analysis of ligand displacement binding data has extended the range to subnanomolar potencies, permitting a detailed characterization of the ΔH and ΔS contributions to the ΔG of binding (41). Despite the theoretical development of this ligand displacement ITC approach, it is not widely used. The thermodynamic profiles of compound binding to VEGFR2-CD and VEGFR2-CD/JM were evaluated by the ligand displacement ITC method (Table 3) to reveal an interesting observation. For both protein constructs, the change in enthalpy (ΔH) upon inhibitor binding contributes the major part of the overall ΔG of binding of these highly potent molecules. However, differential entropic effects were observed for inhibitor binding to the VEGFR2-CD/JM protein relative to the VEGFR2-CD protein. Compound binding to VEGFR2-CD is accompanied by an unfavorable entropic change, which offsets in part the large, favorable change in enthalpy. Conversely, when the JM domain is present, the increase in potency observed relative to the catalytic domain is not the result of a more favorable ΔH but a more favorable entropic effect. The exact interpretation of binding thermodynamics for protein–ligand interactions can be complicated by large variations in ΔH and ΔS compared to ΔG . More comprehensive biophysical studies on a large set of inhibitors need to be performed to fully evaluate this observation. Nonetheless, the observation indicates that the JM domain may have a role in regulating the catalytic domain.

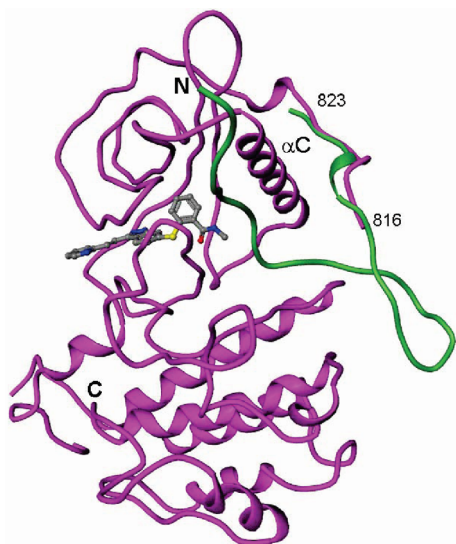


FIGURE 7: Model of VEGFR2 JM position. The position of the JM domain in the crystal structure of autoinhibited cKit (PDB entry 1T45 (green)) superimposed onto the crystal structure of axitinib bound to nonphosphorylated VEGFR2-CD (magenta). Axitinib is depicted in ball and stick representation.

Structural Model of VEGFR2-CD/JM. A likely position and function of the VEGFR2 JM domain may be inferred by overlaying published crystal structures of axitinib bound to nonphosphorylated VEGFR2-CD (55) and crystal structures of other PDGFR family members containing the JM domain (24, 26, 28, 55, 56). An overlay of the structure of the nonphosphorylated VEGFR2-CD bound to axitinib (55) and the nonphosphorylated cKit kinase apoenzyme structure containing the JM domain (26, 55, 56) was modeled (Figure 7). In autoinhibited cKit, the JM domain extends into the kinase active site, located in the cleft between the N- and C-terminal domains of the kinase, preventing the kinase from adopting a catalytically active conformation. After emerging from the catalytic domain cleft, the cKit JM forms a loop and then folds over the top of α -helix C. Residues 816–823 in the VEGFR2-CD axitinib complex fold over α -helix C very similarly to the corresponding residues in cKit. The model suggests that residues N-terminal to residue 816 in VEGFR2 may also follow a path similar to autoinhibited cKit. In this position, the JM domain may act like a “clasp” to hold the N- and C-terminal domains fixed, minimizing dynamics associated with entropy. In contrast, without the JM present, the protein may be more dynamic, particularly by rotations at the hinge region linking the N- and C-terminal domains. This hypothesis can help to explain the unfavorable entropy observed on the binding of compounds to the VEGFR2-CD protein as the binding of these inhibitors in the cleft between the N- and C-terminal domains is likely to stabilize the protein and change the protein conformational equilibrium more in favor of one conformation. In contrast, with the JM present and acting as a “clasp”, the protein is stabilized toward a single conformation associated with low dynamics, and inhibitor binding in the hinge site does not have such a large entropic penalty. Support for this hypothesis is provided by the DSC studies that show a significant effect of the JM domain on the thermal stability of the VEGFR2 catalytic domain, which supports the idea of a change in the overall folded state or ensemble of states of the protein. In addition, the analytical size exclusion chromatography studies showed that the larger VEGFR2-CD/JM protein runs “smaller”

than VEGFR2-CD, which may be evidence for a more compact conformation. While other possible contributions to the observed binding thermodynamics, such as the effect of disruption of water molecules and the uptake or release of protons coupled to compound binding, cannot be ruled out, the modeling and thermal stability data together provide support for the hypothesis that the underlying effect of the JM is on the dynamics of the protein.

CONCLUSION

Regulatory mechanisms of receptor tyrosine kinases are important for controlling many cellular processes. Evidence for a facile intramolecular autophosphorylation reaction of the JM domain may be critical to understanding the biology of VEGFR2. The presence of the JM domain of VEGFR2 has a substantial effect on inhibitor binding to the catalytic domain of VEGFR2, and potencies determined with the combined CD/JM construct correlated better with cellular potency. These studies reinforce the importance of selecting the proper protein construct for mechanistic studies of RTK and their inhibitors.

ACKNOWLEDGMENT

We gratefully acknowledge Steve Grant for helpful discussions on the manuscript.

REFERENCES

1. Board, R., and Jayson, G. C. (2005) Platelet-derived growth factor receptor (PDGFR): a target for anticancer therapeutics. *Drug Resist. Updates* 8, 75–83.
2. Fischer, B., Marinov, M., and Arcaro, A. (2007) Targeting receptor tyrosine kinase signalling in small cell lung cancer (SCLC): what have we learned so far?. *Cancer Treat. Rev.* 33, 391–406.
3. Sun, L., and McMahon, G. (2000) Inhibition of tumor angiogenesis by synthetic receptor tyrosine kinase inhibitors. *Drug Discov. Today* 5, 344–353.
4. Zwick, E., Bange, J., and Ullrich, A. (2002) Receptor tyrosine kinases as targets for anticancer drugs. *Trends Mol. Med.* 8, 17–23.
5. Folkman, J. (2007) Angiogenesis: an organizing principle for drug discovery?. *Nat. Rev. Drug Discov.* 6, 273–286.
6. Ellis, L. M., and Hicklin, D. J. (2008) VEGF-targeted therapy: mechanisms of anti-tumour activity. *Nat. Rev.* 8, 579–591.
7. Roskoski, R., Jr. (2008) VEGF receptor protein-tyrosine kinases: structure and regulation. *Biochem. Biophys. Res. Commun.* 375, 287–291.
8. Hu-Lowe, D. D., Zou, H. Y., Grazzini, M. L., Hallin, M. E., Wickman, G. R., Amundson, K., Chen, J. H., Rewolinski, D. A., Yamazaki, S., Wu, E. Y., McTigue, M. A., Murray, B. W., Kania, R. S., O'Connor, P., Shalinsky, D. R., and Bender, S. L. (2008) Nonclinical antiangiogenesis and antitumor activities of axitinib (AG-013736), an oral, potent, and selective inhibitor of vascular endothelial growth factor receptor tyrosine kinases 1, 2, 3. *Clin. Cancer Res.* 14, 7272–7283.
9. Choueiri, T. K. (2008) Axitinib, a novel anti-angiogenic drug with promising activity in various solid tumors. *Curr. Opin. Invest. Drugs* 9, 658–671.
10. McTigue, M. A., Wickersham, J. A., Pinko, C., Showalter, R. E., Parast, C. V., Tempczyk-Russell, A., Gehring, M. R., Mroczkowski, B., Kan, C. C., Villafranca, J. E., and Appelt, K. (1999) Crystal structure of the kinase domain of human vascular endothelial growth factor receptor 2: a key enzyme in angiogenesis. *Structure* 7, 319–330.
11. Dougher-Vermazen, M., Hulmes, J. D., Bohlen, P., and Terman, B. I. (1994) Biological activity and phosphorylation sites of the bacterially expressed cytosolic domain of the KDR VEGF-receptor. *Biochem. Biophys. Res. Commun.* 205, 728–738.
12. Takahashi, T., Yamaguchi, S., Chida, K., and Shibuya, M. (2001) A single autophosphorylation site on KDR/Flk-1 is essential for VEGF-A-dependent activation of PLC-gamma and DNA synthesis in vascular endothelial cells. *EMBO J.* 20, 2768–2778.

13. Kendall, R. L., Rutledge, R. Z., Mao, X., Tebben, A. J., Hungate, R. W., and Thomas, K. A. (1999) Vascular endothelial growth factor receptor KDR tyrosine kinase activity is increased by autophosphorylation of two activation loop tyrosine residues. *J. Biol. Chem.* 274, 6453–6460.
14. Dayanir, V., Meyer, R. D., Lashkari, K., and Rahimi, N. (2001) Identification of tyrosine residues in vascular endothelial growth factor receptor-2/FLK-1 involved in activation of phosphatidylinositol 3-kinase and cell proliferation. *J. Biol. Chem.* 276, 17686–17692.
15. Meyer, R. D., Dayanir, V., Majnoun, F., and Rahimi, N. (2002) The presence of a single tyrosine residue at the carboxyl domain of vascular endothelial growth factor receptor-2/FLK-1 regulates its autophosphorylation and activation of signaling molecules. *J. Biol. Chem.* 277, 27081–27087.
16. Sakurai, Y., Ohgimoto, K., Kataoka, Y., Yoshida, N., and Shibuya, M. (2005) Essential role of Flk-1 (VEGF receptor 2) tyrosine residue 1173 in vasculogenesis in mice. *Proc. Natl. Acad. Sci. U.S.A.* 102, 1076–1081.
17. Rahimi, N. (2006) Vascular endothelial growth factor receptors: molecular mechanisms of activation and therapeutic potentials. *Exp. Eye Res.* 83, 1005–1016.
18. Hubbard, S. R. (2004) Juxtamembrane autoinhibition in receptor tyrosine kinases. *Nat. Rev. Mol. Cell. Biol.* 5, 464–471.
19. Parast, C. V., Mroczkowski, B., Pinko, C., Misialek, S., Khambatta, G., and Appelt, K. (1998) Characterization and kinetic mechanism of catalytic domain of human vascular endothelial growth factor receptor-2 tyrosine kinase (VEGFR2 TK), a key enzyme in angiogenesis. *Biochemistry* 37, 16788–16801.
20. Hubbard, S. R., and Miller, W. T. (2007) Receptor tyrosine kinases: mechanisms of activation and signaling. *Curr. Opin. Cell Biol.* 19, 117–123.
21. Huse, M., and Kuriyan, J. (2002) The conformational plasticity of protein kinases. *Cell* 109, 275–282.
22. Rosnet, O., and Birnbaum, D. (1993) Hematopoietic receptors of class III receptor-type tyrosine kinases. *Crit. Rev. Oncog.* 4, 595–613.
23. Binns, K. L., Taylor, P. P., Sicheri, F., Pawson, T., and Holland, S. J. (2000) Phosphorylation of tyrosine residues in the kinase domain and juxtamembrane region regulates the biological and catalytic activities of Eph receptors. *Mol. Cell. Biol.* 20, 4791–4805.
24. Griffith, J., Black, J., Faerman, C., Swenson, L., Wynn, M., Lu, F., Lippke, J., and Saxena, K. (2004) The structural basis for autoinhibition of FLT3 by the juxtamembrane domain. *Mol. Cell* 13, 169–178.
25. Li, S., Covino, N. D., Stein, E. G., Till, J. H., and Hubbard, S. R. (2003) Structural and biochemical evidence for an autoinhibitory role for tyrosine 984 in the juxtamembrane region of the insulin receptor. *J. Biol. Chem.* 278, 26007–26014.
26. Mol, C. D., Dougan, D. R., Schneider, T. R., Skene, R. J., Kraus, M. L., Scheibe, D. N., Snell, G. P., Zou, H., Sang, B. C., and Wilson, K. P. (2004) Structural basis for the autoinhibition and STI-571 inhibition of c-Kit tyrosine kinase. *J. Biol. Chem.* 279, 31655–31663.
27. Mol, C. D., Lim, K. B., Sridhar, V., Zou, H., Chien, E. Y., Sang, B. C., Nowakowski, J., Kassel, D. B., Cronin, C. N., and McRee, D. E. (2003) Structure of a c-kit product complex reveals the basis for kinase transactivation. *J. Biol. Chem.* 278, 31461–31464.
28. Schubert, C., Schalk-Hihi, C., Struble, G. T., Ma, H. C., Petrounia, I. P., Brandt, B., Deckman, I. C., Patch, R. J., Player, M. R., Spurlino, J. C., and Springer, B. A. (2007) Crystal structure of the tyrosine kinase domain of colony-stimulating factor-1 receptor (cFMS) in complex with two inhibitors. *J. Biol. Chem.* 282, 4094–4101.
29. Backer, J. M., Kahn, C. R., Cahill, D. A., Ullrich, A., and White, M. F. (1990) Receptor-mediated internalization of insulin requires a 12-amino acid sequence in the juxtamembrane region of the insulin receptor beta-subunit. *J. Biol. Chem.* 265, 16450–16454.
30. Wybenga-Groot, L. E., Baskin, B., Ong, S. H., Tong, J., Pawson, T., and Sicheri, F. (2001) Structural basis for autoinhibition of the Ephb2 receptor tyrosine kinase by the unphosphorylated juxtamembrane region. *Cell* 106, 745–757.
31. Huse, M., Chen, Y. G., Massague, J., and Kuriyan, J. (1999) Crystal structure of the cytoplasmic domain of the type I TGF beta receptor in complex with FKBP12. *Cell* 96, 425–436.
32. Till, J. H., Becerra, M., Watty, A., Lu, Y., Ma, Y., Neubert, T. A., Burden, S. J., and Hubbard, S. R. (2002) Crystal structure of the MuSK tyrosine kinase: insights into receptor autoregulation. *Structure* 10, 1187–1196.
33. Ma, Y., Cunningham, M. E., Wang, X., Ghosh, I., Regan, L., and Longley, B. J. (1999) Inhibition of spontaneous receptor phosphorylation by residues in a putative alpha-helix in the KIT intracellular juxtamembrane region. *J. Biol. Chem.* 274, 13399–13402.
34. Chan, P. M., Ilangumaran, S., La Rose, J., Chakrabarty, A., and Rottapel, R. (2003) Autoinhibition of the kit receptor tyrosine kinase by the cytosolic juxtamembrane region. *Mol. Cell. Biol.* 23, 3067–3078.
35. Kania, R. S., Bender, S. L., Borchardt, A. J., Cripps, S. J., Hua, Y., Johnson, M. D., Theodore Otto Johnson, J., Luu, H. T., Palmer, C. L., Reich, S. H., Tempczyk-Russell, A. M., Teng, M., Thomas, C., Varney, M. D., Wallace, M. B., and Collins, M. R. (2001) Indazole compounds and pharmaceutical compositions for inhibiting protein kinases, and methods for their use, U.S. Patent 6,534,524.
36. Borchardt, A. J., Kania, R. S., and Palmer, C. L. (2003) Indazole compounds and pharmaceutical compositions for inhibiting protein kinases, and methods for their use, U.S. Patent 7,053,107.
37. Collins, M., Cripps, S., Deal, J., Kania, R. S., Lou, J., He, M., Palmer, C. L., III, W. H. R., and Zhou, R. (2003) Benzofused heterozyrly amide derivatives of thienopyridines useful as therapeutic agents, pharmaceutical compositions including the same, and methods for their use, U.S. Patent 6,869,962.
38. Morrison, J. F. (1969) Kinetics of the reversible inhibition of enzyme-catalysed reactions by tight-binding inhibitors. *Biochim. Biophys. Acta* 185, 269–286.
39. Murphy, D. J. (2004) Determination of accurate KI values for tight-binding enzyme inhibitors: an in silico study of experimental error and assay design. *Anal. Biochem.* 327, 61–67.
40. Wiseman, T., Williston, S., Brandts, J. F., and Lin, L. N. (1989) Rapid measurement of binding constants and heats of binding using a new titration calorimeter. *Anal. Biochem.* 179, 131–137.
41. Sigurskjold, B. W. (2000) Exact analysis of competition ligand binding by displacement isothermal titration calorimetry. *Anal. Biochem.* 277, 260–266.
42. Morton, T. A., and Myska, D. G. (1998) Kinetic analysis of macromolecular interactions using surface plasmon resonance biosensors. *Methods Enzymol.* 295, 268–294.
43. Copeland, R. A. (2000) Use of tight binding inhibitors to determine active enzyme concentration, in *Enzymes* (2nd Ed.). A Practical Introduction to Structure, Mechanism, and Data Analysis (Copeland, R. A., Ed.) pp 313–315, Wiley-VCH, New York.
44. Rich, R. L., Hoth, L. R., Geoghegan, K. F., Brown, T. A., LeMotte, P. K., Simons, S. P., Hensley, P., and Myska, D. G. (2002) Kinetic analysis of estrogen receptor/ligand interactions. *Proc. Natl. Acad. Sci. U.S.A.* 99, 8562–8567.
45. Murray, B. W., Padrique, E. S., Pinko, C., and McTigue, M. A. (2001) Mechanistic effects of autophosphorylation on receptor tyrosine kinase catalysis: enzymatic characterization of Tie2 and phospho-Tie2. *Biochemistry* 40, 10243–10253.
46. Gotoh, N., Tojo, A., Hino, M., Yazaki, Y., and Shibuya, M. (1992) A highly conserved tyrosine residue at codon 845 within the kinase domain is not required for the transforming activity of human epidermal growth factor receptor. *Biochem. Biophys. Res. Commun.* 186, 768–774.
47. Cunningham, S. A., Arrate, M. P., Brock, T. A., and Waxham, M. N. (1997) Interactions of FLT-1 and KDR with phospholipase C gamma: identification of the phosphotyrosine binding sites. *Biochem. Biophys. Res. Commun.* 240, 635–639.
48. Greggio, E., Zambrano, I., Kaganovich, A., Beilina, A., Taymans, J. M., Daniels, V., Lewis, P., Jain, S., Ding, J., Syed, A., Thomas, K. J., Baekelandt, V., and Cookson, M. R. (2008) The Parkinson disease-associated leucine-rich repeat kinase 2 (LRRK2) is a dimer that undergoes intramolecular autophosphorylation. *J. Biol. Chem.* 283, 16906–16914.
49. Joseph, R. E., Fulton, D. B., and Andreotti, A. H. (2007) Mechanism and functional significance of Itk autophosphorylation. *J. Mol. Biol.* 373, 1281–1292.
50. Tummino, P. J., and Copeland, R. A. (2008) Residence time of receptor-ligand complexes and its effect on biological function. *Biochemistry* 47, 5481–5492.
51. Copeland, R. A., Pompliano, D. L., and Meek, T. D. (2006) Drug-target residence time and its implications for lead optimization. *Nat. Rev. Drug Discov.* 5, 730–739.
52. Ghose, A. K., Herbertz, T., Pippin, D. A., Salvino, J. M., and Mallamo, J. P. (2008) Knowledge based prediction of ligand binding modes and rational inhibitor design for kinase drug discovery. *J. Med. Chem.* 51, 5149–5171.
53. Hess-Stumpp, H., Haberey, M., and Thierauch, K. H. (2005) PTK 787/ZK 222584, a tyrosine kinase inhibitor of all known VEGF receptors, represses tumor growth with high efficacy. *ChemBioChem* 6, 550–557.

54. Amino, N., Ikeyama, Y., Yamano, M., Kuromitsu, S., Tajima, K., Samizu, K., Hisamichi, H., Matsuhisa, A., Shirasuna, K., Kudoh, M., and Shibasaki, M. (2006) YM-359445, an orally bioavailable vascular endothelial growth factor receptor-2 tyrosine kinase inhibitor, has highly potent antitumor activity against established tumors. *Clin. Cancer Res.* 12, 1630–1638.
55. Bender, S. L., Kania, R. S., and McTigue, M. A. (2004) Crystal structure of human VEGFR2 kinase domain-ligand complexes and use of the atomic coordinates in drug discovery, in *WO 2004/092217 A1*.
56. van der Geer, P., Hunter, T., and Lindberg, R. A. (1994) Receptor protein-tyrosine kinases and their signal transduction pathways. *Annu. Rev. Cell Biol.* 10, 251–337.